HOKKAIDO UNIVERSITY

Title	Relative contributions of external forcing factors to circulation and hydrographic properties in a micro-tidal bay
Author(s)	Yoon, Seokjin; Kasai, Akihide
Citation	Estuarine coastal and shelf science, 198, 225-235 https://doi.org/10.1016/j.ecss.2017.09.017
Issue Date	2017-11-05
Doc URL	http://hdl.handle.net/2115/76013
Rights	© 2017. This manuscript version is made available under the CC-BY-NC-ND 4.0 license http://creativecommons.org/licenses/by-nc-nd/4.0/
Rights(URL)	http://creativecommons.org/licenses/by-nc-nd/4.0/
Type	article (author version)
File Information	Kasai ECSS.pdf

Instructions for use

Hokkaido University Collection of Scholarly and Academic Papers : HUSCAP

Relative contributions of external forcing factors to circulation and hydrographic properties in a micro-tidal bay

Seokjin Yoon[a,b,*] and Akihide Kasai[a,b]

[a] Faculty of Fisheries Sciences, Hokkaido University, 3-1-1 Minato, Hakodate, Hokkaido 041-8611, Japan

[b] Core Research for Evolutionary Science and Technology (CREST), Japan Science and Technology Agency, Gobancho, Chiyoda-ku, Tokyo 102-0076, Japan

* Corresponding author. Address: Faculty of Fisheries Sciences, Hokkaido University, 3-1-1 Minato, Hakodate, Hokkaido 041-8611, Japan. Tel.: +81 138 40 8807.

E-mail address: seokjin.yoon@gmail.com (S. Yoon).

Abstract

The dominant external forcing factors influencing estuarine circulation differ among coastal environments. A three-dimensional regional circulation model was developed to estimate external influence indices and relative contributions of external forcing factors such as external oceanic forcing, surface heat flux, wind stress, and river discharge to circulation and hydrographic properties in Tango Bay, Japan. Model results show that in Tango Bay, where the Tsushima Warm Current passes offshore of the bay, under conditions of strong seasonal winds and river discharge, the water temperature and salinity are strongly influenced by surface heat flux and river discharge in the surface layer, respectively, while in the middle and bottom layers both are mainly controlled by open boundary conditions. The estuarine circulation is comparably influenced by all external forcing factors, the strong current, surface heat flux, wind stress, and river discharge. However, the influence degree of each forcing factor varies with temporal variations in external forcing factors as: the influence of open boundary conditions is higher in spring and early summer when the stronger current passes offshore of the bay, that of surface heat flux reflects the absolute value of surface heat flux, that of wind stress is higher in late fall and winter due to strong seasonal winds, and that of river discharge is higher in early spring due to snow-melting and summer and early fall due to flood events.

Keywords:
Estuarine circulation; External forcing factor; External influence index; Regional circulation model; Wakasa Bay; Tango Bay

1. Introduction

Regions of freshwater influence (ROFI; Simpson et al., 1993) form transition zones between oceanic and riverine environments and are one of the most productive marine ecosystems (McLusky and Elliott, 2004). ROFI ecosystems are driven by complex interactions of physical and biochemical processes, and the physical processes such as estuarine circulation have a major influence on the biochemical processes through the transport of nutrients and organisms (Mann and Lazier, 2005). The physical processes are under the combined influences of external forcing: oceanic (such as tides, waves, and the intrusion of high salinity water), atmospheric (such as surface heat flux and wind stress), and riverine (such as river discharge) forcing (reviewed by Uncles, 2002). Extensive studies on the influences of external forcing on ROFIs have shown that they are dominated by forcing factors such as tides (e.g., Sylaios et al., 2006), wind stress (e.g., Geyer, 1997; Cariniello et al., 2011), and river discharge (e.g., Liu et al., 1997), or a balance between/among these forcing factors (e.g., Niedda and Greppi, 2007). The dominant forcing factor changes in different ROFI environments, and the degree of influence of each forcing factor varies with temporal variations in external forcing factors (reviewed by Llebot et al., 2014).

Wakasa Bay (Fig. 1), located in western Honshu Island, Japan, is one of the largest bays along the Japanese coast of the Sea of Japan. The bottom depth is 50 to 100 m over a large section of the bay, being deepest in the mouth of the bay. It is well known that the tide is small in the Sea of Japan, and the tidal range is less than 50 cm at the Maizuru tidal station of the Japan Meteorological Agency. The Tsushima Warm Current enters the Sea of Japan through the Tsushima Straits and flows at depths shallower than 200 m offshore of Wakasa Bay (Hase et al., 1999). Strong northwesterly winds prevail in late fall and winter, whereas in summer winds are weak except during sporadic events such as typhoons. Two large rivers, the Yura River and the Kita River, flow into the bay. The ROFI of the Yura River (Tango Bay; Fig. 1c) is located in the southwestern part of Wakasa Bay and is connected through two passages, the northern (NP) and eastern (EP) passages, which are east and south of the Kammuri Island (ca. 22 km from the river mouth), respectively. This ROFI is an important spawning and nursery ground for several fishes such as seabass (*Lateolabrax japonicus*) and flounder (*Paralichthys olivaceus*), and the estuarine circulation plays an important role in the transport of eggs and larvae (Fuji et al., 2010; Fuji et al., 2014; Watanabe et al., 2014).

Several physical oceanographic surveys in and around Wakasa Bay have been conducted. Yamagata et al. (1984) and Umatani et al. (1986) reported the intrusion of a warmer and less saline water mass, derived from the Tsushima Warm Current, into Wakasa Bay in summer.

Hashimoto (1982) and Hara et al. (1992) reported the occurrence of anticyclonic circulation in Wakasa Bay in summer caused by the Tsushima Warm Current. Kumaki et al. (2005) and Kumaki et al. (2012) reported the occurrence of a strong coastal current related to the increase and decrease in water temperature around the Tango Peninsula after and before the passage of a typhoon, respectively. Although previous studies mainly focused on short-term fluctuations, Itoh et al. (2016) conducted a long-term mooring and hydrographic survey at four stations (corresponding to St. 1−4 shown in Fig. 1c) between 2012 and 2014 in order to clarify the seasonal circulation pattern in Tango Bay and the forces driving this flow. As their results show, the anticyclonic circulation flows across the bay with the inflow and outflow at the eastern and northern openings, respectively, and this flow intensifies in winter. They carried out correlation analysis between mooring data (velocity and salinity) and forcing factors (river discharge, wind speed and direction, and Tsushima Warm Current index), and concluded that the circulation in the bay is strongly affected by seasonal winds and the Tsushima Warm Current.

Numerical simulations also have been conducted in coastal regions including Wakasa Bay. Igeta et al. (2007) and Kumaki et al. (2012) used a three-dimensional hydrodynamic model with a horizontal resolution of 1 km to explain the generation mechanism of the strong coastal current around the Tango Peninsula before and after the passage of a typhoon. The model results showed that the “before” current was generated by continuous strong easterly winds (Kumaki et al., 2012), and the “after” one was caused by the backwash from waves breaking in the swash zone (Igeta et al., 2007). While both previous models considered only wind stress as forcing, Hirose et al. (2016) developed a three-dimensional coastal ocean model (called DR_C) with a horizontal resolution of 1.5 km considering a realistic open boundary condition obtained from a regional data assimilation system (Hirose et al., 2013), surface heat flux, wind stress, and river discharges. The polygon in Fig. 1a indicates the DR_C model domain. The DR_C simulated rapid changes in the coastal current mostly associated with strong wind events, and the model results showed good agreement with in-situ velocity observations. The model also simulated the anticyclonic circulation in Wakasa Bay, which was developed from a vortex separated from the Tango Peninsula.

Physical processes in an open bay, which is influenced by river water, are generally complex and highly localized (Simpson, 1997; Itoh et al., 2016). Although previous studies reported that Wakasa Bay is significantly influenced by the Tsushima Warm Current and wind stress, the relative contribution of each forcing factor has not been evaluated as compared with the other factors such as surface heat flux and river discharge. In this study using a three-dimensional regional circulation model, therefore, we evaluated the relative contributions of external forcing factors such as external oceanic forcing, surface heat flux, wind stress, and river discharge to circulation and hydrographic properties (i.e., water temperature, salinity, and velocity) in Tango Bay on a monthly and annual time scale.

2. Model configuration

The Princeton Ocean Model (POM), which is a three-dimensional numerical ocean model (Mellor, 2002), has been widely applied to coastal areas and estuaries (e.g., Oey et al., 1985; Xue et al., 2000; Wong et al., 2003; Yoon et al., 2013). The sigma coordinate system, in which the vertical coordinate is scaled on the water column depth, is useful to simulate significant topographical variabilities in estuaries and over continental shelf breaks and slopes (Mellor, 2002).

In this study, the model (POM) was configured for Wakasa Bay. The model domain is shown in Fig. 1b (100 km × 63 km). The horizontal grid was discretized by 199 × 125 lattice points with a resolution of 500 m, and there were 20 non-uniform vertical layers with a finer resolution near the surface being σ = 0.000, −0.007, −0.017, −0.027, −0.041, −0.061, −0.088, −0.116, −0.150, −0.190, −0.245, −0.306, −0.374, −0.442, −0.510, −0.578, −0.646, −0.714, −0.796, −0.891, and −1.000. Time steps were 1 second for the external mode and 30 seconds for the internal mode. Main parameter values of the POM are given in Table 1.

The bottom topography was obtained from the J-EGG500 (JODC-Expert Grid data for Geography-500 m) provided by the Japan Oceanographic Data Center (JODC). In addition, a high-resolution (100 m in horizontal resolution) topographic survey was conducted in and around Tango Bay to define the topography.

The open boundary conditions were obtained from the DR_C. The hourly surface elevation, water temperature, salinity, and horizontal velocities of the DR_C were transferred to the open boundary of the POM after linear interpolation in time and space.

The surface meteorological conditions were obtained from the NCEP/DOE Reanalysis with a resolution of 250 km and the operational meso-scale model (MSM) with a resolution of 5 km of the Japan Meteorological Agency. The hourly solar radiation at the sea surface, converted from the daily downward solar radiation flux of the NCEP/DOE Reanalysis using the NOAA Solar Calculator, and the hourly air temperature, cloud cover, relative humidity, and wind vector of the MSM were linearly interpolated in time and space into the resolutions of the POM.

The surface heat flux (Q), i.e., total downward flux of heat across the ocean surface, was estimated based on Haney (1971) as $Q = QS - (QB + QH + QE)$. The QS is the downward flux of solar radiation which penetrates the sea surface as $QS = G(1-\alpha)$, where G is the solar radiation at the sea surface and α is the albedo of the sea surface. The QB, QH, and QE are the net upward flux of longwave radiation, sensible heat, and latent heat, respectively, as $QB = Q^{*}\sigma_{sb}T_s^{\,4}$, $QH = \rho_a C_d \left|\vec{U}_{wind}\right| C_p (T_s - T_a)$, and $QE = \rho_a C_d \left|\vec{U}_{wind}\right| L(q_s - q_a)$, where Q^{*} is an empirical function of air temperature, cloud cover, and relative humidity, σ_{sb} is the Stefan-Boltzmann constant, T_s is the sea surface temperature, ρ_a is the air density, C_d is the variable drag coefficient proposed by Deacon and Webb (1962) as $C_d = (1 + 0.07\left|\vec{U}_{wind}\right|) \times 10^{-3}$, $\vec{U}_{wind}$ is the wind velocity vector, C_p is the specific heat of air at constant pressure, L is the latent heat of vaporization, q_s is the saturation specific humidity, and q_a is the specific humidity. The eastward and northward wind stress components were estimated as $\tau_x = \rho_a C_d W_x \left|W_x\right|$ and $\tau_y = \rho_a C_d W_y \left|W_y\right|$, respectively, where W_x and W_y are the eastward and northward wind speed, respectively.

The river stage (H_{riv}) and discharge (Q_{riv}) of the Yura River and the Kita River have been monitored by the Ministry of Land, Infrastructure, Transport and Tourism (MLIT), Japan. The H_{riv} is expressed relative to the mean sea level of Tokyo Bay, Japan. The hourly river discharge was estimated from the hourly river stage based on the relationship between H_{riv} (m) and Q_{riv} (m^3 s^{-1}), obtained from the MLIT, as $Q_{riv} = 80.76 \times (H_{riv} + 2.19)^2$ when $H_{riv} \le 0.00$, $Q_{riv} = 22.44 \times (H_{riv} + 4.15)^2$ when $0.00 < H_{riv} \le 3.27$, and $Q_{riv} = 77.09 \times (H_{riv} + 0.73)^2$ when $3.27 < H_{riv}$ for the Yura River, and

$Q_{riv} = 37.14 \times (H_{riv} - 2.75)^2$ for the Kita River. The river discharge was assumed as the downward vertical velocity at the surface layer of each river inflow grid cell in the POM based on Oey (1996) with linear interpolation in time. The water temperature of river water was estimated as a function of air temperature based on the observation in the Yura River from April 2006 to March 2008 (unpublished data), and the salinity was set to zero.

The simulation was started from 00:00 January 1, 2012 under the initial condition interpolated from the DR_C, and run for three years (to 24:00 December 31, 2014). For model stabilization, the year of 2012 was run twice. For model validation, the model was compared with observations obtained from mooring systems, which were deployed at stations 1–4 (Fig. 1c) between 2012 and 2014 (Itoh et al., 2016). The water temperature and salinity, measured using the conductivity-temperature (CT) sensor at the depth of 0.5, 1.5, 3.5, and 28 m of St. 1 (bottom depth of 29 m), 54 m of St. 2 (61 m), 62 m of St. 3 (70 m), and 72.5 m of St. 4 (76 m), and the velocity, measured using the ADCP on the seabed at Sts. 3 and 4, were used. Sigma coordinate model results were interpolated to the observation depths.

To evaluate the seasonal relative contributions of external forcing factors such as open boundary conditions (BC), surface heat flux (HF), wind stress (WS), and river discharge (RD) to the circulation and hydrographic properties in Tango Bay, five climatological control scenarios were designed as Table 2. We used climatological values for external forcing factors during the period 2012 to 2014. The CLIM was defined as a standard scenario modeled under four climatological external forcing conditions, BC, HF, WS, and RD, and the other four CTRLs (Table 2) were simulated under the conditions of CLIM without a specific external forcing as: the CTRL_BC without the BC (i.e., sponge boundary conditions), the CTRL_HF without the HF, the CTRL_WS without the WS, and the CTRL_RD without the

RD. The control scenarios were run for two years, and the first year was used as the spin-up period. From the monthly mean model results in Tango Bay bounded by the NP and EP lines shown in Fig. 1c, the external influence index (EII) of an external forcing (F) was calculated as:

$$EII_F = \sqrt{\frac{\sum_{i=1}^{N}(X_i - Y_i)^2}{N-1}} ,$$

where subscript F indicates the open boundary conditions (BC), surface heat flux (HF), wind stress (WS), or river discharge (RD), X_i and Y_i are the monthly mean model results of CTRL and CLIM in the “wet” grid cells, respectively, and N is the number of the model results. The number of “wet” grid cells was 1129 horizontally and 20 vertically (totally 22580), in which there were 22580 water temperature data points, 22580 salinity data points, and 41900 horizontal velocity data points. For example, the EII of BC, EII_{BC}, on water temperature was calculated using the water temperatures of CTRL_BC (X_i) and CLIM (Y_i) with the number of the model results of 22580. For example, when the water temperature decreases (or increases) 1 °C uniformly over Tango Bay under the condition without the BC compared with that of CLIM, the EII_{BC} on water temperature is approximately equal to 1. In this study, the relative contribution of an external forcing factor (F) was defined as “the percentage of EII_F in the summation of all EIIs” and symbolized as $\%EII_F$:

$$\%EII_F = \frac{EII_F}{EII_{BC} + EII_{HF} + EII_{WS} + EII_{RD}} \times 100 .$$

3. External forcing factors

Figure 2 shows the four major external forcing factors, the Tsushima Warm Current, surface heat flux and wind stress averaged over the entire model domain, and river discharges of the Yura River and Kita River in Wakasa Bay. The Tsushima Warm Current Index (TWCI) is represented as the volume flux through the Oki Strait (OS shown in Fig. 1a) simulated by the DR_C. The Tsushima Warm Current flows into the Sea of Japan through the Tsushima Straits, and the nearshore branch passes the Oki Strait before reaching Wakasa Bay. The TWCI exhibits a seasonal change with an increasing trend from winter to summer and sharply decreases in fall. This trend corresponds to the sea level difference between the extreme edges of the Oki Strait (Itoh et al., 2016). The surface heat flux fluctuates sinusoidally with a maximum in June and a minimum in December. The wind stress is strong in late fall and winter due to the strong northwesterly seasonal winds, while weak in summer. Especially the northerly wind dominated in the beginning of 2014. The river discharges fluctuate with high annual and interannual variability, due to rainfall and snowfall. The early spring peaks are associated with the melting of snow, and the two extreme peaks in September 2013 and August 2014 are attributed to heavy rainfall due to typhoons. The annual mean discharges of the Yura River and Kita River were 57 m^3 s^{-1} and 15 m^3 s^{-1}, respectively.

The western open boundary (WOB shown in Fig. 1b) is the main route of inflow of the Tsushima Warm Current, because the nearshore branch flows eastward or northeastward along the Japanese coast. Therefore, the water temperature and salinity averaged between 0−100 m on the WOB (Figs. 3a−b) are expected to reflect those of the Tsushima Warm Current. The water temperature fluctuates sinusoidally with a maximum in September and a minimum in March. The water temperature was lower in 2014 (September mean of 21.8 °C) compared with the other years (23.8 °C in 2012 and 23.5 °C in 2013). The interannual variation in the water temperature is due to the surface heat flux (August mean of 160 W m^{-2} in 2012, 174 W m^{-2} in 2013, and 133 W m^{-2} in 2014) (Fig. 2b) and is influenced by the original water temperature of the Tsushima Warm Current. The salinity exhibits high seasonality with a maximum in May (monthly mean of 34.5 in 2012 and 2013, and 34.7 in 2014) and a minimum in November (33.5 in all three years). The marked decrease in salinity after June is mainly due to the Changjiang Diluted Water entrained into the Tsushima Warm Current (Itoh et al., 2016). The seasonal variation in the eastward velocity averaged between 0−100 m on the WOB (Fig. 3c) corresponds to that in the TWCI (Fig. 2a). The offshore oceanic water entered through the WOB (i.e., the positive eastward velocity shown in Fig. 3c) flows out through the northern open boundary that is the positive northward velocity (the summation of both velocities) shown in Fig. 3d. The northern open boundary is divided into two equal-width parts, the northwestern (NWOB) and northeastern (NEOB) open boundaries. The northward velocities averaged between 0−100 m on the NWOB and NEOB shown in Fig. 3d represent the main path of the Tsushima Warm Current from WOB to NEOB (i.e., the speed is faster on NEOB) in spring and early summer and to NWOB (i.e., faster on NWOB) in late summer.

4. Model validation

Figure 4 shows the simulated salinities with horizontal velocity vectors at the depths of 1 and 50 m in Wakasa Bay in January (representing winter), June (representing high salinity early summer), and August (representing low salinity late summer) 2013. The Tsushima Warm Current flows to the north of the bay, being weak in winter and strong in summer (Fig. 3c). In summer, the strong offshore current generates an anticyclonic circulation in the bay, and the modeled circulation corresponds to the circulation observed by Hashimoto (1982) and

Hara et al. (1992). The main path of the Tsushima Warm Current in June is different from that in August, and this leads to the different circulation pattern in the bay. The anticyclonic circulation is generated in the center of the bay in June, but it shifts to the northeastern part in August, when the cyclonic circulation is remarkable in the southern part of the bay. The circulation pattern at the depth of 50 m in Tango Bay as the inflow and outflow at the eastern and northern passages, respectively, corresponds to the observed circulation reported by Itoh et al. (2016). The circulation strengthens in winter, especially in the lower layers, while it weakens in summer (see detail in section 5.1). Freshwater from the Yura River generates a salinity gradient eastward along the coast near the surface. At the depth of 50 m, the river-induced salinity gradient is indistinctive, and the salinity exhibits a gradual gradient from the coast to the open sea. The intrusion of the less saline water mass into Wakasa Bay reported by Yamagata et al. (1984) and Umatani et al. (1986) is clearly shown in late summer, after the marked decrease in the offshore salinity (Fig. 3b).

The model results were compared with observational data at stations 1–4 (shown in Fig. 1c) obtained from Itoh et al. (2016). Figure 5 shows the comparison between daily mean model results and observations for water temperature and salinity at the depths of 0.5, 1.5, 3.5, and 28 m of St. 1, 54 m at St. 2, 62 m of St. 3, and 72.5 m of St. 4 throughout the observation periods. The modeled water temperature and salinity show a fairly good agreement with observed values, although the salinity data scatter increases in the low salinity range (< 30). The temporal variations in water temperature, salinity, and velocity at representative positions were also compared between the model results and observations. Time series data derived from the model results and observational data for water temperature and salinity in the surface layer (at the depth of 0.5 m) at St. 1 (the shallowest and nearest observation station to the mouth of the Yura River) and in the bottom layer (72.5 m) at St. 4 (the deepest observation station) are shown in Fig. 6, and those for velocity in the surface (0.5 m), middle (29 m), and bottom (59 m) layers at Sts. 3 (nearly the central point of the northern passage of Tango Bay) and 4 (nearly the central point of the eastern passage of the bay) are shown in Fig. 7. As well as water temperature and salinity, the modeled velocities also showed good agreement with the observations, although there is a trivial discrepancy during summer. These results indicate our model can represent the real hydrographic conditions fairly well in Tango Bay. Therefore, it is appropriate to evaluate the relative contributions of the external forcing factors to the circulation and hydrographic properties in the bay, using this model. Details of the circulation and hydrographic properties in Tango Bay are described in section 5.1.

5. Model results

5.1. Circulation and hydrographic properties in Tango Bay

The water temperature and salinity in Tango Bay fluctuate seasonally (Fig. 6). The seasonal variation in water temperature in the bottom layer is almost the same as the offshore water temperature (Fig. 3a). The water temperature fluctuates sinusoidally with a maximum in August to September and a minimum in February to March. The maximum and minimum occur slightly earlier at St. 1 than those on the WOB under the influence of the surface heat flux and river discharge (i.e., the shallow area is easy to heat/cool). The seasonal variation in salinity shows a different pattern between the surface and bottom layers. The surface salinity responds sensitively to the Yura River discharge and fluctuates dramatically during the spring snow-melting and flood periods. The maximum occurs in May to June in the low river discharge season, and the minimum occurs during the highest Yura River discharge in each year (i.e., in March 2012, September 2013, and August 2014). However, the bottom salinity follows almost the same fluctuation as the offshore salinity (Fig. 3b). Two minima occurred in September and November every year. The peaks are not the influence of the Yura River discharge, but the intrusion of less saline offshore water. The maximum and minimum occur in May to June and in November, respectively, corresponding to the offshore salinity.

The velocities in the surface layer show a different behavior from velocities in the middle and bottom layers at Sts. 3 and 4 (Fig. 7). In the surface layer, the flow speed varies irregularly, whereas the flow direction changes seasonally as: the predominant direction is northeastward at St. 3 and southwestward at St. 4 in winter, and southwestward at St. 3 and eastward at St. 4 in summer. On the other hand, in the middle and bottom layers, the flow speed varies seasonally with a maximum in winter and a minimum in late spring/early summer, whereas the flow direction is almost constant as the predominant direction is northward (i.e., out away from the bay) at St. 3 and westward (i.e., into the bay) at St. 4. This indicates that the offshore water enters Tango Bay from the eastern passage and exits to the northern passage. The circulation is stronger in winter and weaker in late spring/early summer, as shown in Fig. 4.

5.2. Relative contributions of external forcing factors to the hydrographic conditions in Tango Bay

Table 3 shows the external influence indices (EIIs) and relative contributions (%EIIs) of external forcing factors in Tango Bay bounded by the NP and EP lines shown in Fig. 1c on an annual time scale. The bay is divided into six sub-domains as: two horizontally (areas the bottom depth (D) is ≤ 50 m near the shore and > 50 m further from the shore) and three vertically (the surface (the first; σ = −0.003), middle (the 14th; σ = −0.476), and bottom (the 20th; σ = −0.946) layers), consequently as: (1) D ≤ 50 m and σ = −0.003, (2) D ≤ 50 m and σ = −0.476, (3) D ≤ 50 m and σ = −0.946, (4) D > 50 m and σ = −0.003, (5) D > 50 m and σ = −0.476, and (6) D > 50 m and σ = −0.946.

The influence of external forcing factors on the water temperature is higher in order of BC ($\%EII_{BC}$ = 47%), HF ($\%EII_{HF}$ = 37%), RD ($\%EII_{RD}$ = 12%), and WS ($\%EII_{WS}$ = 4%) in the entire domain of Tango Bay. This indicates BC and HF are the most important external forcing factors to determine the water temperature in the bay. While $\%EII_{BC}$ is higher in the middle and bottom layers than in the surface layer, $\%EII_{HF}$, $\%EII_{WS}$, and $\%EII_{RD}$ are higher in the surface layer. In the surface layer of the inshore area (D ≤ 50 m), the most influential external forcing factor is HF ($\%EII_{HF}$ = 50), while BC in the middle and bottom layers ($\%EII_{BC}$ is 46 and 51, respectively). In the surface layer of the nearshore area (D > 50 m), both BC ($\%EII_{BC}$ = 43%) and HF ($\%EII_{HF}$ = 42%) are influential, and the influence of BC is most marked ($\%EII_{BC}$ > 80%) in the middle and bottom layers.

The influence of external forcing factors on the salinity is higher for RD ($\%EII_{RD}$ = 68%), BC ($\%EII_{BC}$ = 17%), HF ($\%EII_{HF}$ = 8.3%), and WS ($\%EII_{WS}$ = 7.6%) in the entire domain. RD is the most important external forcing factor to determine the salinity in the inshore area ($\%EII_{RD}$ ≥ 60%) and the surface layer of the nearshore area ($\%EII_{RD}$ = 42%), while in the middle and bottom layers BC is the most important factor ($\%EII_{BC}$ ≥ 70%).

The influence of external forcing factors on the velocity is higher for BC ($\%EII_{BC}$ = 36%), RD ($\%EII_{RD}$ = 22%), WS ($\%EII_{WS}$ = 21%), and HF ($\%EII_{HF}$ = 20%) in the entire domain. The differences among the four external forcing factors are relatively small compared with the water temperature and salinity. In the six sub-domains, %EII ranges from 12 to 45%, smaller than those of the water temperature (2 to 88%) and salinity (3 to 79%). While the water temperature and salinity are mainly affected by one or two external forcing factors, the velocity is affected by all external forcing factors, even if the influence of the HF seems weak intuitively. The influences of RD and BC are relatively predominant in the inshore and nearshore areas, respectively.

Figure 8 shows time series of relative contributions (%EIIs) of external forcing factors in the entire domain of Tango Bay on a monthly time scale. %EII for the water temperature fluctuates considerably depending on the BC and HF. $\%EII_{BC}$ fluctuates with two peaks in early spring and late summer, when the offshore water temperature is at a minimum and a maximum, respectively (Fig. 3a). The influence of HF is smaller than that of BC except in December to January and May to June, when HF is at a minimum and a maximum, respectively (Fig. 2b). This indicates that the offshore water plays a more important role in the cooling and heating of the water in the bay except when the absolute value of HF is close to its maximum. $\%EII_{WS}$ increases in winter due to the strong seasonal wind, but is weak and stable throughout the year relatively to that of the other factors. $\%EII_{RD}$ is higher than $\%EII_{HF}$ in February and March, when the cold freshwater flows into the bay due to the melting of snow.

%EII for the salinity is directly related to $\%EII_{RD}$ throughout the year. $\%EII_{RD}$ is lower from May to June, corresponding to the low river discharge season (Fig. 2d). Although the river discharge is higher in summer and fall, $\%EII_{RD}$ is slightly higher in spring. The reason is that the offshore salinity is higher in spring than in summer and fall (Fig. 3b), and the influence of RD is larger when the river (the salinity is zero) flows into the higher salinity bay. $\%EII_{BC}$ fluctuates with two peaks in late spring and late fall, when the offshore salinity is the maximum and the minimum, respectively (Fig. 3b). $\%EII_{WS}$ and $\%EII_{HF}$ are higher in winter and summer, respectively, but both are smaller than $\%EII_{BC}$ throughout the year.

%EII for the velocity is distributed evenly among the four external forcing factors, compared with that to the water temperature and salinity. $\%EII_{BC}$ is higher from March to July, when the inward velocity on the WOB is faster compared with other months (i.e., the Tsushima Warm Current is stronger), and the offshore velocity is faster on the NEOB than on the NWOB (i.e., the main path of the Tsushima Warm Current is toward NEOB) (Figs. 3c−d, e.g. Figs. 4c−d). On the other hand, $\%EII_{BC}$ is lower in August although the inward velocity on the WOB is also faster in August, because the outward velocity is faster on the NWOB than on the NEOB (e.g., Fig. 4e−f). In other words, when the open ocean seawater entering through the WOB flows out through the NWOB, the influence on the nearshore circulation is larger than that when it flows out through the NEOB. $\%EII_{HF}$ is at the maximum in June, when HF is the maximum, and at minima in March and October, when the absolute value of HF is close to 0 (Fig. 2b). $\%EII_{WS}$ is at its maximum in February, when the southward wind stress is the maximum. (Fig. 2c). Although the eastward wind stress is at its maximum in December (which value is higher than in February), $\%EII_{WS}$ is not high. This indicates that the influence of wind on the nearshore circulation is affected by the wind direction as: the southward wind has greater influence than the eastward wind. $\%EII_{RD}$ is above 20% except during the low river discharge season in May and June.

6. Discussion and conclusions

While Itoh et al. (2016) concluded that the circulation in Tango Bay is strongly influenced by the Tsushima Warm Current and seasonal winds, our model results showed that the relative contributions of open boundary conditions, surface heat flux, wind stress, and river discharge to the velocity field are comparable in the bay, although that of open boundary conditions is slightly higher than those of the other factors. Itoh et al. (2016) considered three forcing factors of the Tsushima Warm Current, wind, and river and conducted correlation analysis between the three forcing factors and the salinity and velocity observed in the bay. The water temperature and surface heat flux were not taken into consideration, and thus the influence of surface heat flux was omitted. The surface heat flux generating a thermal gradient plays an important role in estuarine circulation (Simpson, 1997; Burchard and Hofmeister, 2008). The influence of surface heat flux has been overlooked when external forcing factors are evaluated (e.g., Geyer, 1997; Liu et al., 1997; Sylaios et al., 2006; Itoh et al., 2016), because it intuitively seems weaker than the other external forcing factors, such as tides, wind stress, and river discharge. In this study, we considered the open boundary conditions as an external oceanic forcing factor. The open boundary conditions such as water temperature, salinity, and velocity obtained from the DR_C (Hirose et al., 2016) contain not only the Tsushima Warm Current but also atmospheric forcing factors, such as surface heat flux and wind stress in the open sea. Consequently, the relative contribution of open boundary conditions is likely to have been overestimated compared with that of the Tsushima Warm Current, while those of surface heat flux and wind stress are likely to have been underestimated, because the influence of surface heat flux and wind stress in the open sea was included in that of open boundary conditions. Despite of the possibility of underestimation, the relative contribution of surface heat flux was only slightly lower than that of open boundary conditions. This indicates that the surface heat flux is as influential as open boundary conditions and wind stress on the estuarine circulation in Tango Bay.

Itoh et al. (2016) reported that the influence of river discharge on the velocity field is only observed at St. 1 (inshore station) and is weaker than those of the Tsushima Warm Currents and seasonal winds in the entire domain of Tango Bay. However, our model results showed that the relative contribution of river discharge to the velocity in the bay (%EII_{RD} = 22%) is similar to that of wind stress (%EII_{WS} = 21%). Freshwater from the Yura River flows eastward along the coast near the surface (e.g., Fig. 4a), and thus the influence of river discharge is small at Sts. 2–4 (nearshore stations). Therefore, the riverine influence reported by Itoh et al. (2016) would be underestimated compared with our model results, because the ratio of the number of inshore (D ≤ 50 m) data to the number of nearshore (D > 50 m) data for correlation analysis (1/3) is smaller than that in this study (> 1/ 1.8).

Offshore oceanic currents have an important influence on the inshore circulation (Huthnance, 1992; Sánchez-Arcilla and Simpson, 2002). The Tsushima Warm Current passing offshore of Wakasa Bay plays an important role in the circulation and hydrographic properties in Tango Bay (Itoh et al., 2016) as well as in Wakasa Bay (Hashimoto, 1982; Yamagata et al., 1984; Umatani et al., 1986; Hara et al., 1992). Our model results showed that open boundary conditions play the most important role in the circulation and hydrographic properties in Tango Bay. Although the relative contribution of open boundary conditions is likely to be higher than that of the Tsushima Warm Current because the influence of surface heat flux and wind stress in the open sea was included in that of open boundary conditions, the influence of open boundary conditions is likely to reflect that of the Tsushima Warm Current because open boundary conditions reflect the Tsushima Warm Current (see detail in section 3).

This study evaluated the relative contributions of the four major external forcing factors of the external oceanic forcing, surface heat flux, wind stress, and river discharge to circulation and hydrographic properties (i.e., water temperature, salinity, and velocity) in Tango Bay using a three-dimensional regional circulation model. The dominant external forcing factor influencing estuarine circulation changes in different estuarine environments. In an extremely shallow lagoon with a mean depth of 0.7 m, the dominant forcing factor is tide even in the micro-tidal regime with a tidal range of 0.1 to 0.4 m (Sylaios et al., 2006). In shallow micro-tidal estuaries with a depth < 4 m and a tidal range < 0.5 m, the dominant forcing factor is wind stress due to strong wind forcing (Geyer, 1997) or river discharge due to strong and episodic freshwater inflow (Liu et al., 1997). We conclude that in Tango Bay, a micro-tidal ROFI with a mean depth of 50 m and a tidal range < 0.2 m, where a strong current (i.e., Tsushima Warm Current) passes offshore of the bay, under conditions of strong seasonal winds and river discharge, the estuarine circulation (i.e., the circulation in Tango Bay bounded by the NP and EP lines shown in Fig. 1c) is comparably influenced by all external forcing factors, i.e., the offshore current, surface heat flux, wind stress, and river discharge. The degree of influence of each forcing factor varies with temporal variations in external forcing factors. The influence of open boundary conditions is higher in spring and early summer when the stronger current passes offshore of the bay; the surface heat flux reflects the absolute value of surface heat flux; wind stress is higher in late fall and winter due to the strong seasonal winds; and river discharge is higher in early spring due to the snow-melt and summer and early fall due to flood events.

Acknowledgements

This work was financially supported by Core Research for Evolutional Science and Technology (CREST) of Japan Science and Technology Agency (JST) through a research project entitled “Application of environmental DNA for quantitative monitoring of fish community and ecosystem assessment” (JST CREST Grant Number JPMJCR13A2). We thank Dr. N. Hirose for supplying the DR_C model results.

References

Burchard, H., Hofmeister, R., 2008. A dynamic equation for the potential energy anomaly for analyzing mixing and stratification in estuaries and coastal seas. Estuarine, Coastal and Shelf Science 77, 679–687. http://dx.doi.org/10.1016/j.ecss.2007.10.025.

Carniello, L., D’Alpaos, A., Defina, A., 2011. Modeling wind waves and tidal flows in shallow micro-tidal basins. Estuarine, Coastal and Shelf Science 92, 263–276. http://dx.doi.org/10.1016/j.ecss.2011.01.001.

Deacon, E.L., Webb, E.K., 1962. Interchange of properties between sea and air. Small-scale interactions. In: Hill, M.N. (Ed.), The Sea Volume 1. Interscience Publisher, New York, USA, pp. 43–87.

Fuji, T., Kasai, A., Suzuki, K.W., Ueno, M., Yamashita, Y., 2010. Freshwater migration and feeding habits of juvenile temperate seabass *Lateolabrax japonicus* in the stratified Yura River estuary, the Sea of Japan. Fisheries Science 76, 643–652. http://dx.doi.org/10.1007/s12562-010-0258-y.

Fuji, T., Kasai, A., Ueno, M., Yamashita, Y., 2014. Growth and migration patterns of juvenile temperate seabass *Lateolabrax japonicus* in the Yura River estuary, Japan–combination of stable isotope ratio and otolith microstructure analyses. Environmental Biology of Fishes 97, 1221–1232. http://dx.doi.org/10.1007/s10641-013-0209-4.

Geyer, W.R., 1997. Influence of wind on dynamics and flushing of shallow estuaries. Estuarine, Coastal and Shelf Science 14, 713–722. http://dx.doi.org/10.1006/ecss.1996.0140.

Haney, R.L., 1971. Surface thermal boundary condition for ocean circulation models. Journal of Physical Oceanography 1, 241–248. http://dx.doi.org/10.1175/1520-0485(1971)001<0241:STBCFO>2.0.CO;2.

Hara, N., Wada, Y., Ueno, M., Munekiyo, M., 1992. Flow patterns in the western part of Wakasa Bay, Japan Sea, in summer. Umi to Sora 68, 51–62 (in Japanese with English abstract).

Hase, H., Yoon, J.H., Koterayama, W., 1999. The current structure of the Tsushima Warm Current along the Japanese coast. Journal of Oceanography 55, 217–235. http://dx.doi.org/10.1023/A:1007894030095.

Hashimoto, Y., 1982. On the flow conditions of Wakasa Bay and its adjacent seas. Umi to Sora 58, 1–11 (in Japanese with English abstract).

Hirose, N., Kumaki, Y., Kaneda, A., Ayukawa, K., Okei, N., Ikeda, S., Igeta, Y., Watanabe, T., 2016. Numerical simulation of the abrupt occurrence of strong current in the southeastern Japan Sea. Continental Shelf Research 143, 194–205. http://dx.doi.org/10.1016/j.csr.2016.07.005.

Hirose, N., Takayama, K., Moon, J.H., Watanabe, T., Nishida, Y., 2013. Regional data assimilation system extended to the East Asian marginal seas. Umi to Sora 89, 43–51.

Huthnance, J.M., 1992. Extensive slope currents and the ocean-shelf boundary. Progress in Oceanography 29, 161–196. http://dx.doi.org/10.1016/0079-6611(92)90023-S.

Igeta, Y., Kitade, Y., Matsuyama, M., 2007. Numerical experiment on *Kyucho* around the Tango Peninsula induced by Typhoon 0406. Journal of Oceanography 63, 835–847. http://dx.doi.org/10.1007/s10872-007-0071-0.

Itoh, S., Kasai, A., Takeshige, A., Zenimoto, K., Kimura, S., Suzuki, K.W., Miyake, Y., Funahashi, T., Yamashita, Y., Watanabe, Y., 2016. Circulation and haline structure of a microtidal bay in the Sea of Japan influenced by the winter monsoon and the Tsushima Warm Current. Journal of Geophysical Research Oceans 121, 6331–6350. http://dx.doi.org/10.1002/2015JC011441.

Kumaki, Y., Kitade, Y., Tojima, T., 2012. *Mae-Kyucho* along the coast of Tango Peninsula. Oceanography in Japan 21, 201–217 (in Japanese with English abstract).

Kumaki, Y., Ueno, Y., Sobajima, N., Matsuyama, M., 2005. The *Kyucho* current along the Kyoto coast induced by Typhoon 0406. Oceanography in Japan 14, 653–664 (in Japanese with English abstract).

Liu, J.T., Zarillo, G.A., Surak, C.R., 1997. The influence of river discharge on hydrodynamics and mixing in a subtropical lagoon. Journal of Coastal Research 13, 1016–1034.

Llebot, C., Rueda, F.J., Solé, J., Artigas, M.L., Estrada, M., 2014. Hydrodynamic states in a wind-driven microtidal estuary (Alfacs Bay). Journal of Sea Research 85, 263–276. http://dx.doi.org/10.1016/j.seares.2013.05.010.

Mann, K.H., Lazier, R.N., 2005. Dynamics of marine ecosystems: Biological-physical interactions in the oceans. Blackwell Publishing, Oxford, UK.

McLusky, D.S., Elliott, M., 2004. The estuarine ecosystem: ecology, threats and management. Oxford University Press, New York, NY, USA.

Mellor, G.L., 2002. Users guide for a three-dimensional, primitive equation, numerical ocean model, 42 pp., Princeton University, Princeton, NJ, USA (Available at http://www.ccpo.odu.edu/POMWEB/UG.10-2002.pdf).

Niedda, M., Greppi, M., 2007. Tidal, seiche and wind dynamics in a small lagoon in the Mediterranean Sea. Estuarine, Coastal and Shelf Science 74, 21–30. http://dx.doi.org/10.1016/j.ecss.2007.03.022.

Oey, L.Y., Mellor, G.L., Hires, R.I, 1985. A three-dimensional simulation of the Hudson-Raritan Estuary. Part I: Description of the model and model simulations. Journal of Physical Oceanography 15, 1676–1692. http://dx.doi.org/10.1175/1520-0485(1985)015<1676:ATDSOT>2.0.CO;2.

Oey, L.Y., 1996. Simulation of mesoscale variability in the Gulf of Mexico: Sensitivity studies, comparison with observations, and trapped wave propagation. Journal of Physical Oceanography 26, 145–175. https://doi.org/10.1175/1520-0485(1996)026<0145:SOMVIT>2.0.CO;2.

Sánchez-Arcilla, A., Simpson, J.H., 2002. The narrow shelf concept: couplings and fluxes. Continental Shelf Research 22, 153–172. http://dx.doi.org/10.1016/S0278-4343(01)00052-8.

Simpson, J.H., 1997. Physical processes in the ROFI regime. Journal of Marine Systems 12, 3–15. http://dx.doi.org/10.1016/S0924-7963(96)00085-1.

Simpson, J.H., Bos, W.G., Schirmer, F., Souza, A.J., Rippeth, T.P., Jones, S.E., Hydes, D., 1993. Periodic stratification in the Rhine ROFI in the North Sea. Oceanologica Acta 16, 23–32.

Sylaios, G.K., Tsihrintzis, V.A., Akratos, C., Haralambidou, K., 2006. Quantification of water, salt and nutrient exchange processes at the mouth of a Mediterranean coastal lagoon. Environmental Monitoring and Assessment 119, 275–301. http://dx.doi.org/10.1007/s10661-005-9026-3.

Umatani, S., Masunaga, N., Yamagata, T., 1986. Further study of synoptic variability in Wakasa Bay, Japan. Progress in Oceanography 17, 359–373. http://dx.doi.org/10.1016/0079-6611(86)90054-6.

Uncles, R.J., 2002. Estuarine physical processes research: Some recent studies and progress.

Estuarine, Coastal and Shelf Science 55, 829–856. http://dx.doi.org/10.1006/ecss.2002.1032.

Watanabe, K., Kasai, A., Antonio, E.S., Suzuki, K., Ueno, M., Yamashita, Y., 2014. Influence of salt-wedge intrusion on ecological processes at lower trophic levels in the Yura Estuary, Japan. Estuarine, Coastal and Shelf Science 139, 67–77. http://dx.doi.org/10.1016/j.ecss.2013.12.018.

Wong, L.A., Chen, J.C., Xue, H., Dong, L.X., Su, J.L., Heinke, G., 2003. A model study of the circulation in the Pearl River Estuary (PRE) and its adjacent coastal waters: 1. Simulations and comparison with observations. Journal of Geophysical Research 108, 3156. http://dx.doi.org/10.1029/2002JC001451.

Xue, H., Chai, F., Pettigrew, N.R., 2000. A model study of the seasonal circulation in the Gulf of Maine. Journal of Physical Oceanography 30, 1111–1135. http://dx.doi.org/10.1175/1520-0485(2000)030<1111:AMSOTS>2.0.CO;2.

Yamagata, T., Umatani, S., Masunaga, N., Matsuura, T., 1984. Observations of an intrusion of a warmer and less saline water mass into a bay. Continental Shelf Research 3, 475–488. http://dx.doi.org/10.1016/0278-4343(84)90024-4.

Yoon, S., Abe, H., Kishi, M.J., 2013. Responses of Manila clam growth and its food sources to global warming in a subarctic lagoon in Japan. Progress in Oceanography 119, 48–58. http://dx.doi.org/10.1016/j.pocean.2013.06.005.

Figures

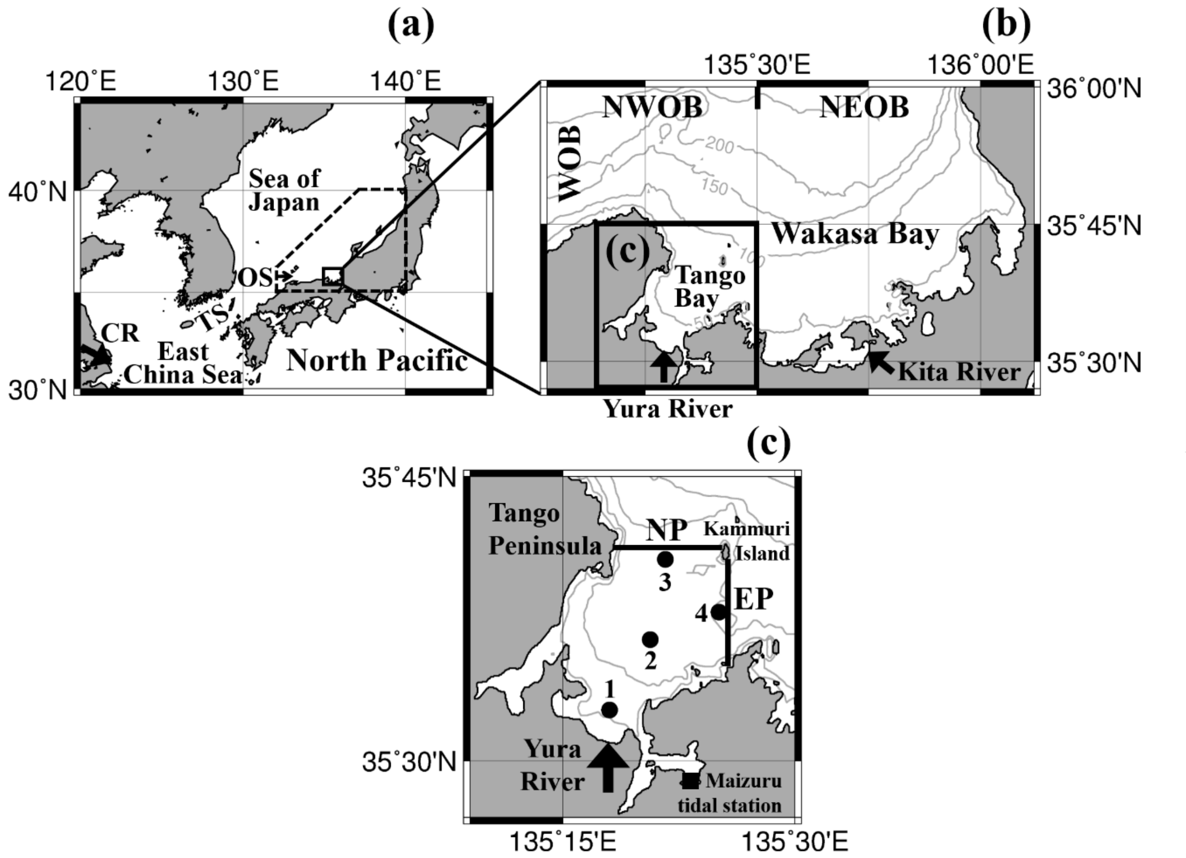

Fig. 1. (a) Location of the study area. CR, TS, and OS indicate Changjiang River, Tsushima Straits, and Oki Strait, respectively, and the dashed polygon indicates the domain of the DR_C model develop by Hirose et al. (2016). (b) Model domain and bathymetry with a contour interval of 50 m. WOB, NWOB, and NEOB indicate the western, northwestern, and northeastern open boundary, respectively. (c) Observation stations with bathymetry with a contour interval of 25 m. Lines NP and EP indicate the northern and eastern passage of Tango Bay, respectively. Numbers represent station numbers.

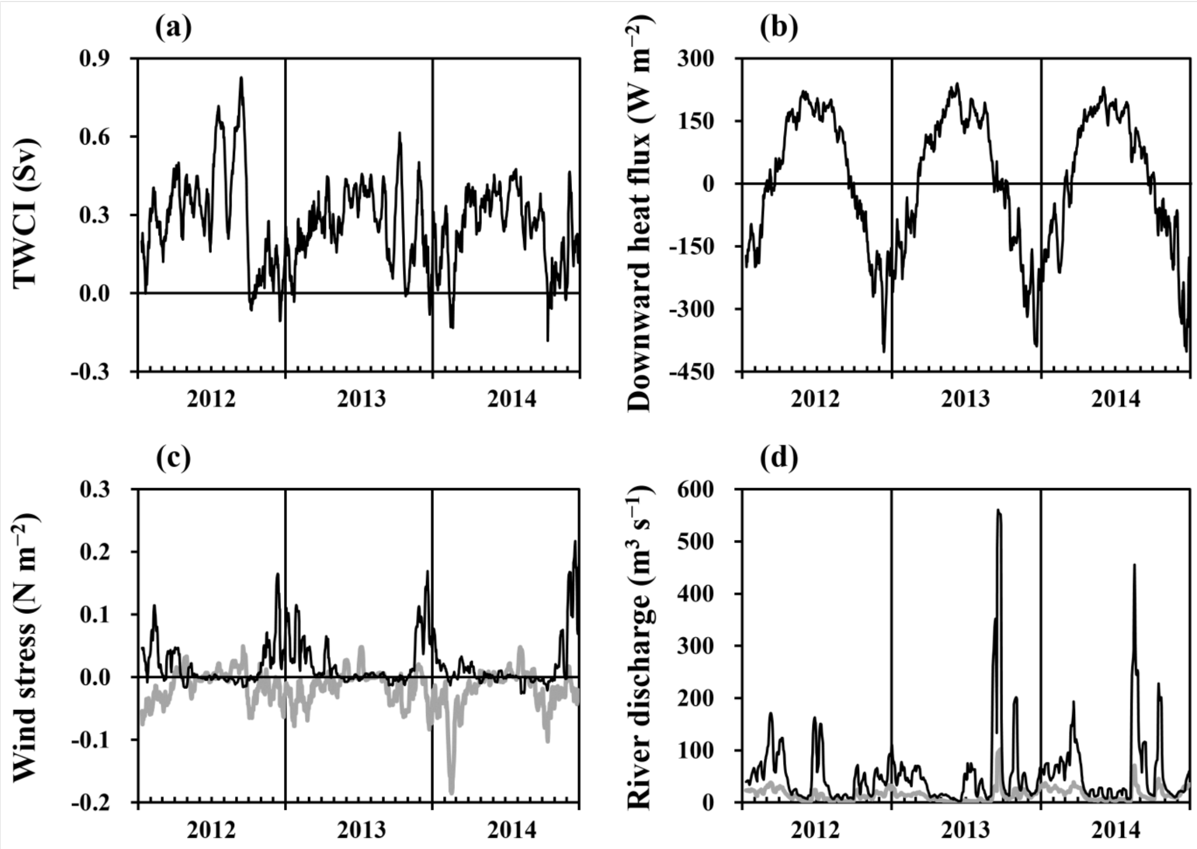

Fig. 2. 10-day moving average time series of (a) Tsushima Warm Current Index (TWCI) (see details in section 3), (b) downward surface heat flux, (c) eastward (black line) and northward (grey line) wind stress averaged over the entire model domain, and (d) the river discharges of the Yura River (black line) and the Kita River (grey line).

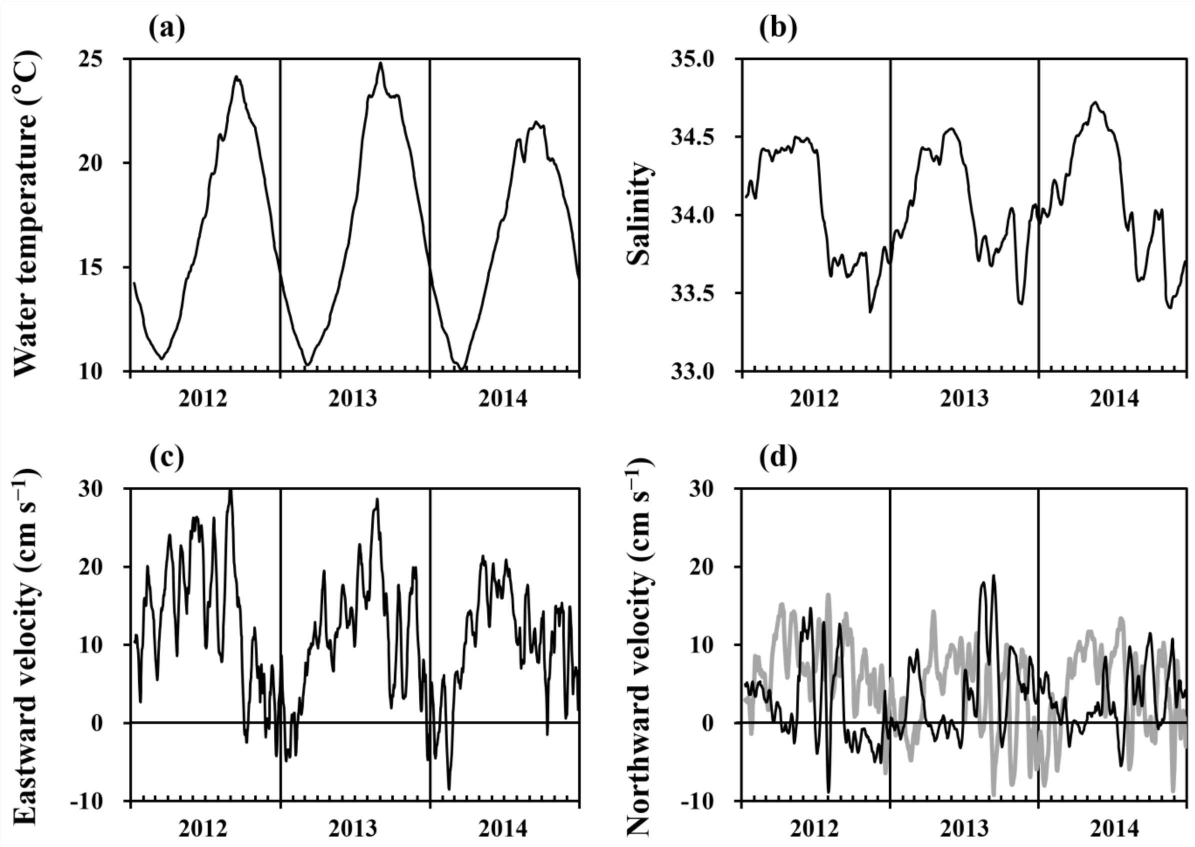

Fig. 3. 10-day moving average time series of (a) water temperature, (b) salinity, and (c) eastward velocity vertically averaged between 0−100 m on the western open boundary (WOB shown in Fig. 1b), and (d) northward velocities on the northwestern (NWOB; black line) and northeastern (NEOB; grey line) open boundary.

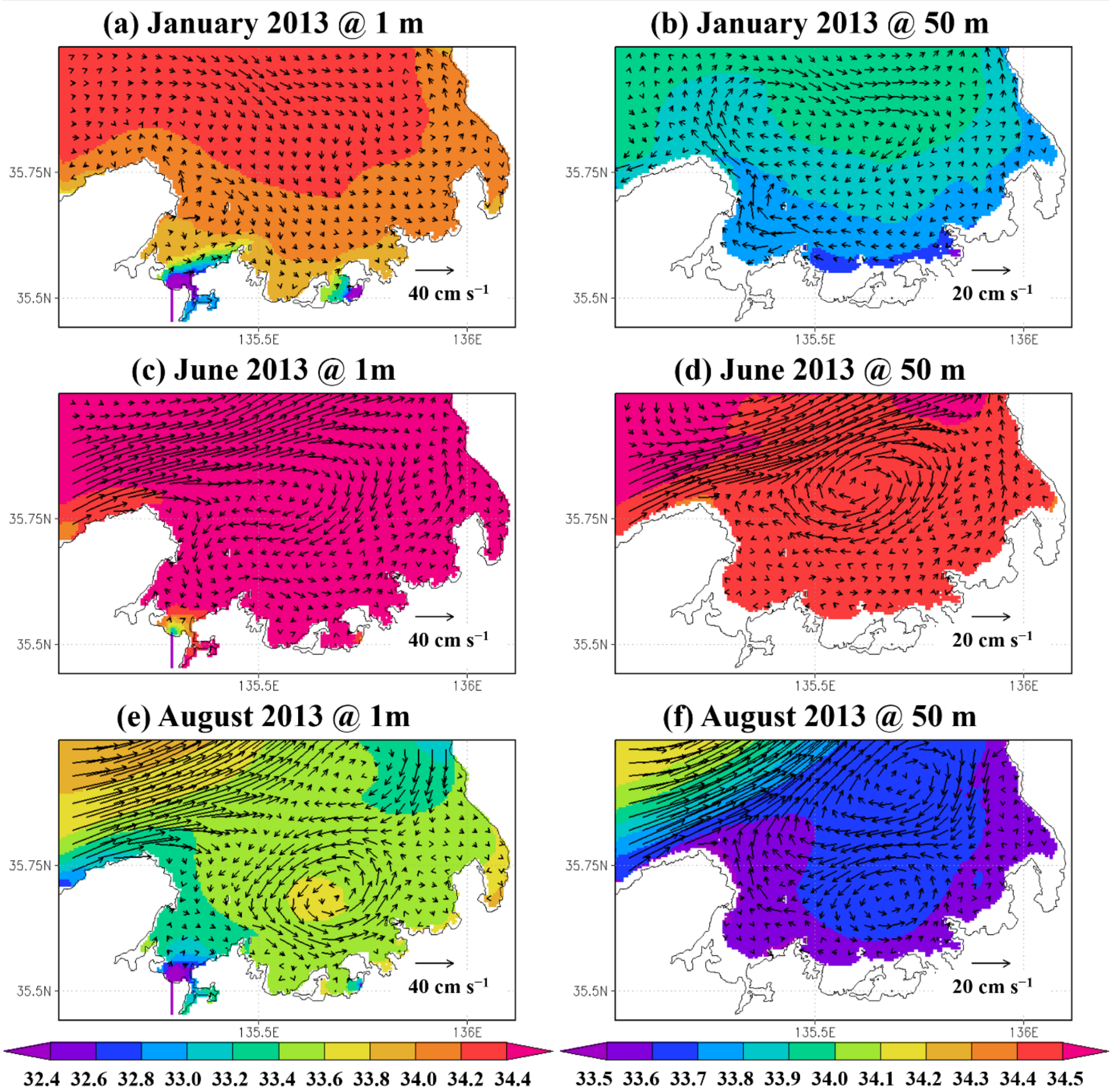

Fig. 4. Simulated monthly mean salinities with horizontal velocity vectors at the depths of 1 and 50 m in Wakasa Bay in January, June, and August 2013. Note the difference of color levels and vector scales between the depths of 1 and 50 m.

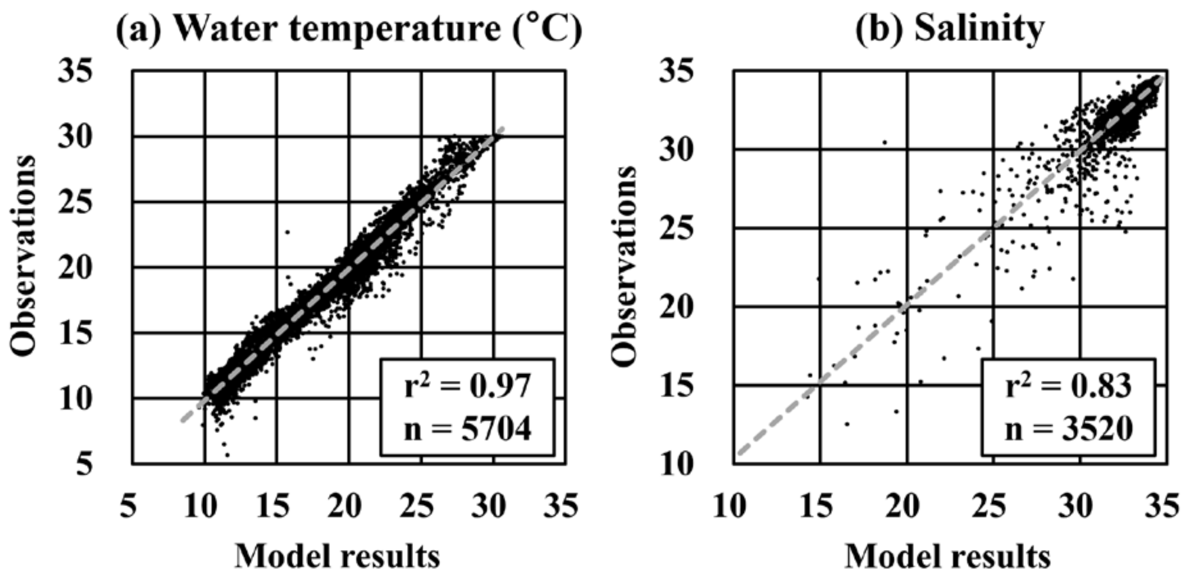

Fig. 5. Scatter plots between model results and observations for water temperature and salinity at the depth of 0.5, 1.5, 3.5, and 28 m at St. 1, 54 m at St. 2, 62 m at St. 3, and 72.5 m at St. 4. These values are expressed as daily mean values. Grey dashed lines indicate the regression lines.

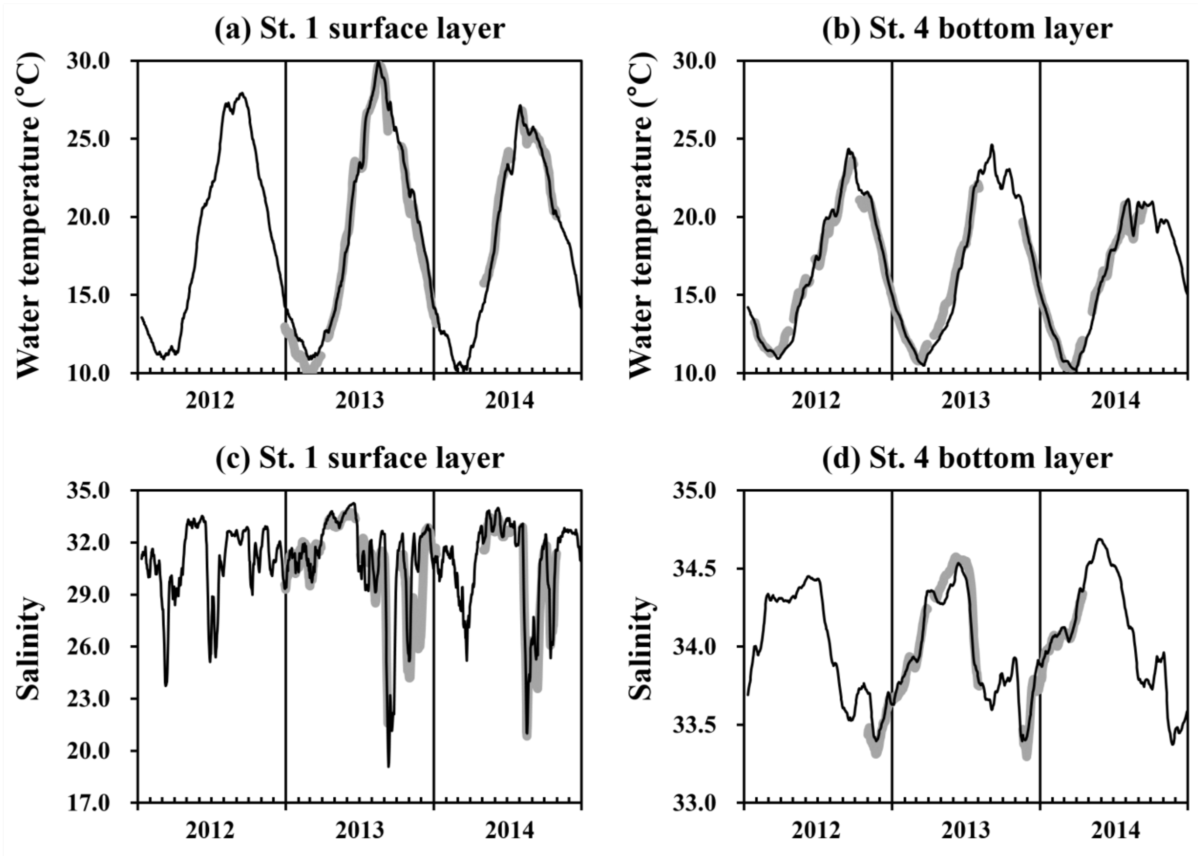

Fig. 6. 10-day moving average time series of model results (black lines) and observations (grey lines) for water temperature and salinity in the surface layer (at the depth of 0.5 m) at St. 1 and the bottom layer (72.5 m) at St. 4 between 2012 and 2014.

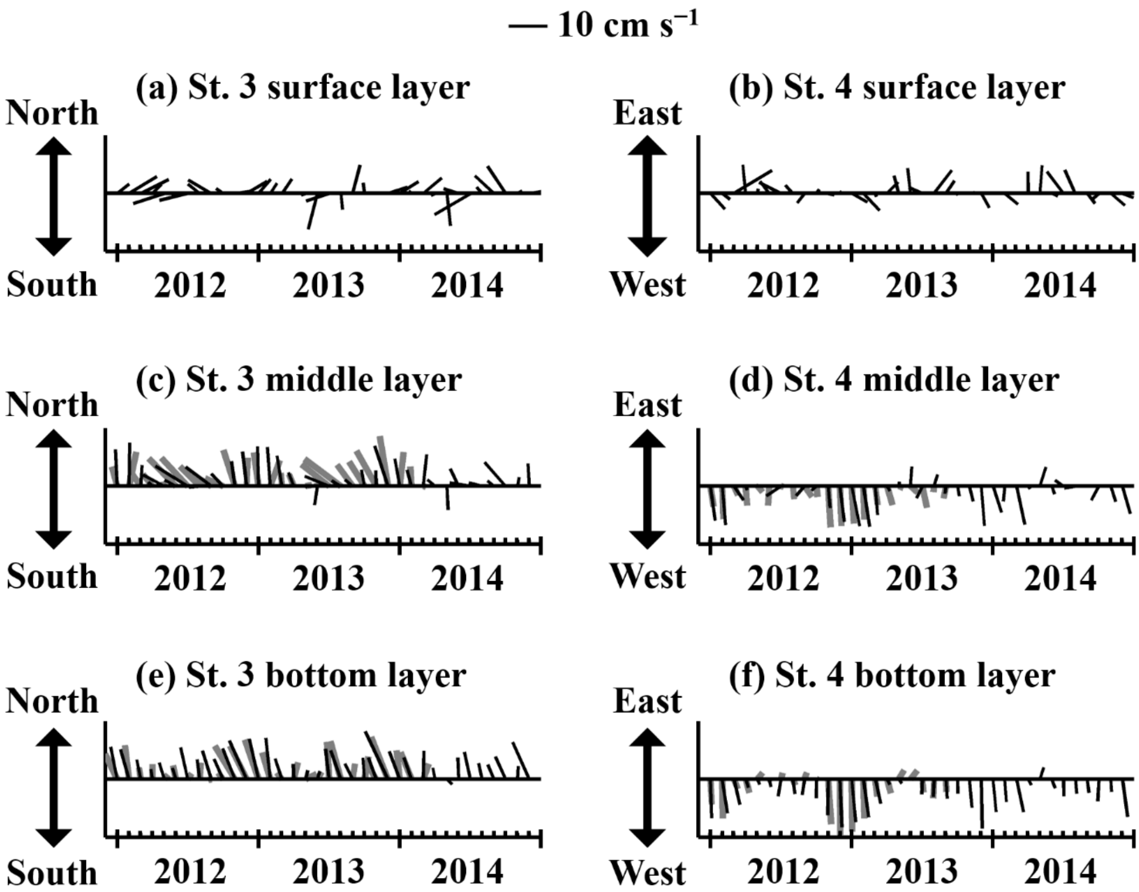

Fig. 7. Stick plots for the modeled (black thin lines) and observed (grey thick lines) velocities in the surface (at the depth of 0.5 m), middle (at the depth of 29 m), and bottom (59 m) layers at Sts. 3 and 4 between 2012 and 2014. The length and direction of each stick represent the speed and direction of the monthly mean velocity. Note the difference of y-axis direction between the two stations: north-south at St. 3 and east-west at St. 4.

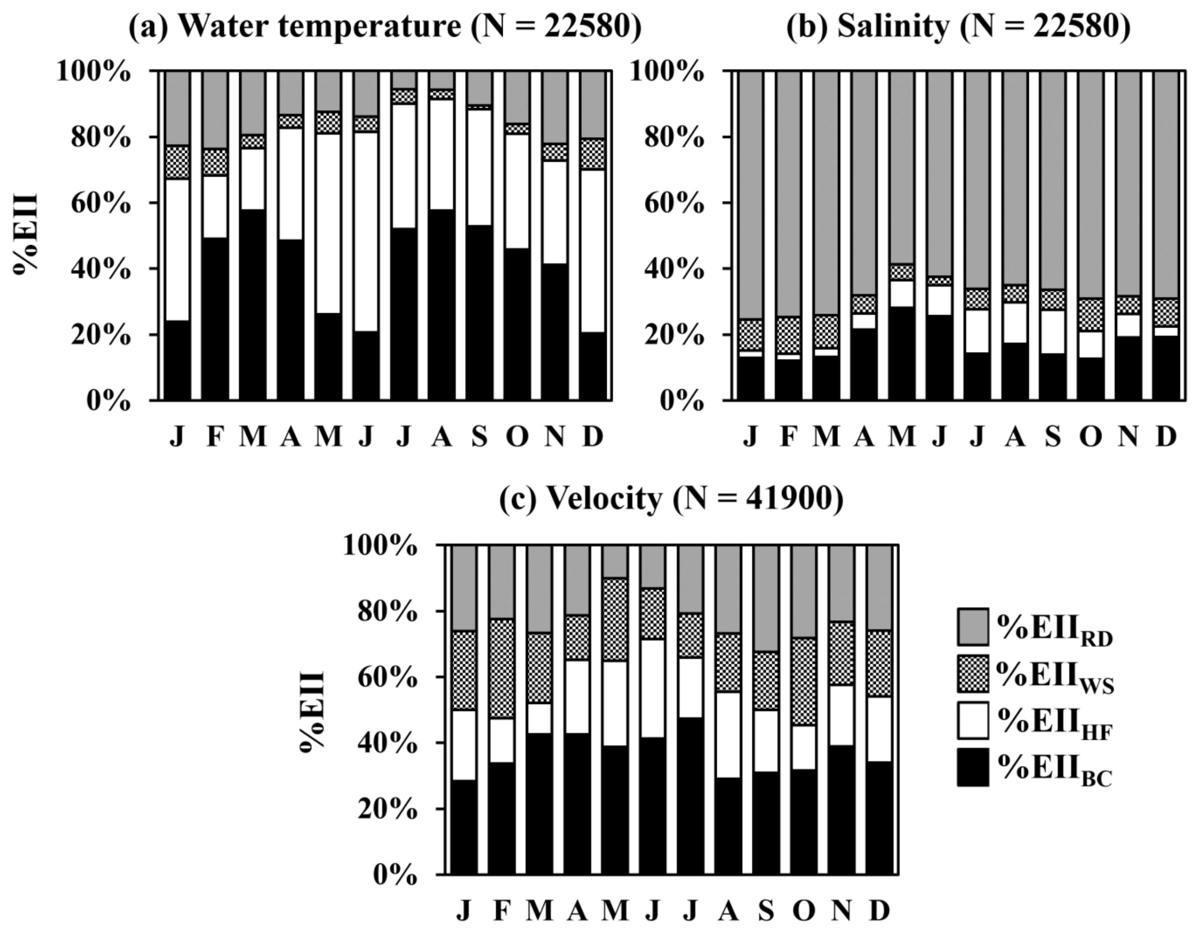

Fig. 8. Monthly relative contributions (%EIIs) of open boundary conditions (%EII_{BC}), surface heat flux (%EII_{HF}), river discharge (%EII_{RD}), and wind stress (%EII_{WS}) to (a) water temperature, (b) salinity, and (c) velocity in the entire model domain of Tango Bay bounded by the NP and EP lines shown in Fig. 1c.

Tables

Table 1 Main parameter values of the Princeton Ocean Model (Mellor, 2002).

Symbol	Parameter description	Value	Unit
nadv	Advection scheme	2	-
nitera	Number of iterations for Smolarkiewicz iterative upstream scheme	2	-
sw	Smoothing parameter for Smolarkiewicz iterative upstream scheme	0.5	-
rhoref	Rerefence density	1025	kg m^{-3}
grav	gravity constant	9.806	m s^{-2}
kappa	von Karman's constant	0.4	-
z0b	Bottom roughness	0.01	m
cbcmin	Minimum bottom friction coefficient	0.0025	-
cbcmax	Maximum bottom friction coefficient	1	-
horcon	Smagorinsky diffusivity coefficient	0.1	-
tprni	Inverse horizontal turbulent Prandtl number	0.1	-
umol	Background vertical diffusivity	0.00002	m^2 s^{-1}
ntp	Water type	2	-
nbct	Surface temperature boundary condition	2	-
nbcs	Surface salinity boundary condition	1	-
ispadv	Step interval during which external mode advective terms are not updated	5	-
smoth	Constant in temporal filter used to prevent solution splitting	0.1	-
alpha	Weight used for surface slope term in external dynamic equation	0.225	-

Table 2 Climatological control scenarios. “Clim.” indicates a climatological value from 2012 to 2014.

Case ID	Open boundary conditions	Heat flux	Wind stress	River discharge
CLIM	Clim.	Clim.	Clim.	Clim.
CTRL_BC	Sponge boundary conditions	Clim.	Clim.	Clim.
CTRL_HF	Clim.	0 W m^{-2}	Clim.	Clim.
CTRL_WS	Clim.	Clim.	0 N m^{-2}	Clim.
CTRL_RD	Clim.	Clim.	Clim.	0 m^3 s^{-1}

Table 3 External influence indices (EIIs) and relative contributions (%EIIs) of external forcing factors, open boundary conditions (BC), surface heat flux (HF), wind stress (WS), and river discharge (RD) to water temperature (T), salinity (S), and velocity (V) in the surface (Sur), middle (Mid), and bottom (Bot) layers of bottom depth (D) ≤ 50 m and > 50 m in Tango Bay bounded by the NP and EP lines shown in Fig. 1c on an annual time scale. Numbers in parentheses indicate %EIIs. The number of data is 5556 for T and S in a layer of D ≤ 50 m, 7992 for T and S in a layer of D > 50 m, 9252 for V in a layer of D ≤ 50 m, and 15888 for V in a layer of D > 50 m.

Compartment	External forcing	Entire	D ≤ 50 m			D > 50 m		
			Sur	Mid	Bot	Sur	Mid	Bot
Temperature	BC	2.47 (47)	2.04 (27)	2.70 (46)	2.79 (51)	1.83 (43)	2.76 (82)	2.60 (88)
	HF	1.93 (37)	3.73 (50)	2.11 (36)	1.80 (33)	1.76 (42)	0.41 (12)	0.18 (6)
	WS	0.22 (4)	0.46 (6)	0.18 (3)	0.13 (2)	0.43 (10)	0.09 (3)	0.11 (4)
	RD	0.64 (12)	1.22 (16)	0.85 (15)	0.75 (14)	0.20 (5)	0.11 (3)	0.06 (2)
Salinity	BC	0.52 (17)	0.60 (10)	0.74 (20)	0.84 (25)	0.36 (23)	0.32 (70)	0.30 (79)
	HF	0.26 (8)	0.45 (7)	0.35 (9)	0.31 (9)	0.14 (9)	0.06 (13)	0.05 (13)
	WS	0.24 (8)	0.63 (10)	0.27 (7)	0.18 (5)	0.39 (25)	0.04 (9)	0.02 (5)
	RD	2.12 (68)	4.49 (73)	2.39 (64)	1.99 (60)	0.65 (42)	0.04 (9)	0.01 (3)
Velocity	BC	3.42 (36)	1.78 (15)	1.24 (28)	0.66 (27)	5.42 (37)	3.44 (45)	1.77 (45)
	HF	1.90 (20)	1.80 (15)	0.95 (22)	0.84 (35)	3.12 (21)	1.59 (21)	0.92 (23)
	WS	1.95 (21)	3.05 (26)	0.90 (21)	0.36 (15)	3.48 (24)	1.49 (20)	0.77 (20)
	RD	2.10 (22)	5.25 (44)	1.30 (30)	0.55 (23)	2.61 (18)	1.05 (14)	0.48 (12)